Mechanical behavior of tungsten–vanadium–lanthana alloys as function of temperature

T. Palacios[1], J.Y. Pastor[2], M.V. Aguirre[1], A. Martín[1], M.A. Monge[2], A. Muñóz[1], R. Pareja[1]

A B S T R A C T

The mechanical behavior of three tungsten (W) alloys with vanadium (V) and lanthana (La_2O_3) additions (W–4%V, W–1%La_2O_3, W–4%V–1%La_2O_3) processed by hot isostatic pressing (HIP) have been compared with pure-W to analyze the influence of the dopants. Mechanical characterization was performed by three point bending (TPB) tests in an oxidizing air atmosphere and temperature range between 77 (immersion tests in liquid nitrogen) and 1273 K, through which the fracture toughness, flexural strength, and yield strength as function of temperature were obtained.

Results show that the V and La_2O_3 additions improve the mechanical properties and oxidation behavior, respectively. Furthermore, a synergistic effect of both dopants results in an extraordinary increase of the flexure strength, fracture toughness and resistance to oxidation compared to pure-W, especially at higher temperatures. In addition, a new experimental method was developed to obtain a very small notch tip radius (around 5–7 μm) and much more similar to a crack through the use of a new machined notch. The fracture toughness results were lower than those obtained with traditional machining of the notch, which can be explained with electron microscopy, observations of deformation in the rear part of the notch tip.

Finally, scanning electron microscopy (SEM) examination of the microstructure and fracture surfaces was used to determine and analyze the relationship between the macroscopic mechanical properties and the micromechanisms of failure involved, depending on the temperature and the dispersion of the alloy.

1. Introduction

Current energy and environmental crises have led to projects to promote the development of environmentally friendly and practically inexhaustible alternative energy renewable sources. Since fusion energy was discovered in 1920 as the true origin of the energy produced by the sun the science and technology community has dreamt of harnessing its power. However, one of the main obstacles faced for the development of this fusion power is finding materials that can withstand extreme operating conditions (e.g., those that will be used to hold the plasma facing components (PFCs) in the International Thermonuclear Experimental Reactor (ITER)).

Due to its characteristics as a refractory material, high melting point, low vapor pressure, low particle impact erosion, thermal conductivity, low radiation damage, and low tritium retention, tungsten (W) a strong candidate for use in the manufacture of PFCs. However, together with these properties, the selected material must maintain a good mechanical performance at high temperature in oxidizing atmosphere conditions. W can significantly improve and modify mechanical behavior by forming solid solutions or dispersion of particles, which allows designing a wide variety of alloys based on specific needs [1].

The long-term target is to achieve a suitable material for using as a component in the divertor. Although this component is going to work in vacuum, one of the accidental scenarios inside the reactor is a loss of vacuum accident. For this reason, it is important to determine the behavior of the materials in case air enters the vacuum vessel and reacts with the PFCs, forming volatile oxides and leading to the oxidation and consequent thermal degradation of the material [2].

2. Materials and experimental methods

2.1. Materials

Three W-alloys with compositions W–4 wt% V, W–1 wt% La_2O_3, and W–4 wt% V–1 wt% La_2O_3 were studied. These target materials were processed from starting powders (the properties of which are

Table 1
Starting powders properties [3].

Powder	Purity (%)	Average particle size (μm)
W	99.9	14
V	99.5	20
La_2O_3	99.9	0.01–0.03

shown in Table 1) using a powder metallurgy route under a high purity Ar atmosphere. The powders were first blended together and then mechanically alloyed in a high-energy planetary mill using tungsten carbide (WC) balls as grinding media.

Afterwards, the powders were canned and degassed inside stainless steel cans. Then, the cans were subjected to a process of consolidation by HIP [3]. This processing synthesized cylindrical alloy samples 30-mm in diameter and 50-mm in length. Prismatic bars of nominal dimensions $1.6 \times 1.6 \times 25\ mm^3$ were prepared from the cylinders by refrigerated electro-discharge machining.

2.2. Experimental methods

Experimental density (ρ_{exp}) of the samples was measured by Archimedes immersion method using high-purity ethanol, whereas theoretical density (ρ_{th}) was calculated using the theoretical densities of each component [3]. Through them, relative density (ρ_r) was calculated to ascertain the porosity of the alloys.

Microhardness of the alloys was measured by performing Vickers (HV) tests following ASTM Standard 384-89 and using loads of 0.98 and 9.8 N with load application time of 12 s. The Impulse Excitation Technique (IET) method, which uses the natural vibration frequencies of the material, was used to measure the dynamic elastic modulus (E_0 IET) [4]. The Oliver and Pharr method [5] and instrumented nanoindentation tests with loads of 0.6 N were used to obtain the elastic modulus (nE) from force–displacement curve and nanohardness (nH). The results obtained can be compared with those obtained with HV tests and IET.

Three point bending (TPB) tests were carried out on smooth and notched prismatic bars using a loading span of 16 and 8.5 mm, respectively. Bars were fractured in a ceramic TPB fixture over the range 77 K using liquid nitrogen immersion to 1273 K, all in oxidant air atmosphere. The bending fixture, connected to the actuator and the frame of the testing machine by ceramic bars, was placed in a high temperature furnace for the tests. Specimens were heated at 50 K/min and held at the test temperature for 15 min before testing. All mechanical tests were performed under stroke control at 100 μm/min. Load and displacement of the load point were continuously monitored during testing using a load cell and a linear variable differential transformer induction transducer, respectively. Three to five samples were used for each material and temperature to ensure test repeatability.

2.2.1. Introducing the notch

To calculate fracture toughness, it was necessary to introduce a controlled crack into the material. Currently, the most reliable way to introduce a controlled crack in metals is through cyclic fatigue, which does not produce plastic damage and, as a result, produces a very small notch tip radius. However, there are limitations to this method, especially if the studied materials are brittle and the amount of material available is limited. An alternative to the fatigue method is to introduce a notch as close as possible to a crack. The most common method is making the notch with a refrigerated diamond disk because it is an easy, fast, and cheap alternative way to cause fatigue. However, some problems arise, such as plastic damage (Fig. 1) or a large notch tip radius around 200 μm. Another method, a diamond wire, produces a smaller notch tip radius (around 70–80 μm), but plastic damage is still problematic.

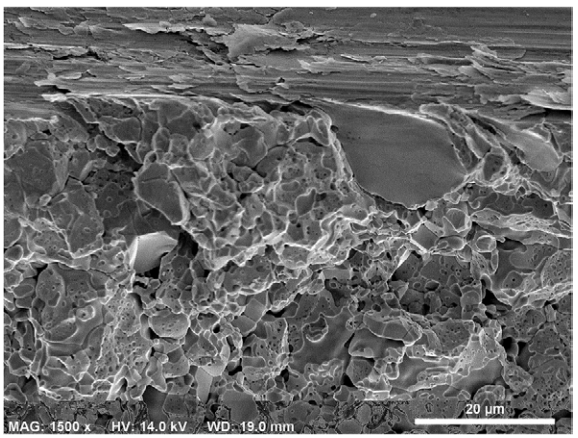

Fig. 1. Plastic damage produced by diamond disk at the notch tip.

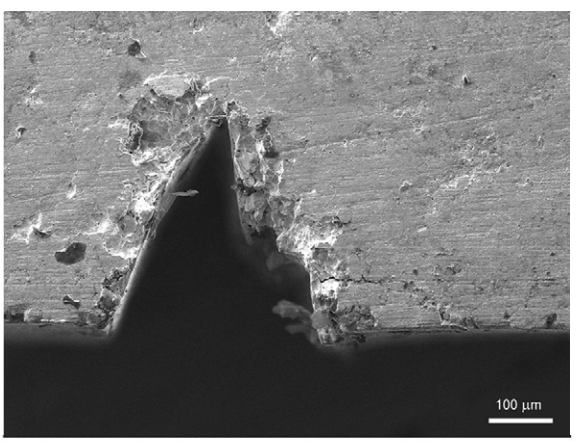

Fig. 2. Notch tip obtained by razor blade notching.

We developed a new experimental method that allows the creation of a notch similar to a crack, with a notch tip radius around 5–7 μm (Fig. 2) and no plastic damage (Fig. 3). The method uses a notching metal razor blade material impregnated with diamond paste. No evidence was found in the literature of a similar application to metals, especially those with low toughness (e.g., W), although a similar method has been applied successfully to other materials with brittle behavior (e.g., ceramics) [6].

This success with ceramic materials is because ceramics are more abrasive than the metallic blade. Consequently, in the machining process of the notch, the blade wastes away with the ceramic abrasive diamond paste causing progressive sharpening of the blade, which generates a notch tip radius around a few microns. In metals, however, materials in contact have a wear resistance of the same order of magnitude which blunts the blade and consequently increases the notch radius. In addition, the blunted blade wears faster than the sample and prevents creation of sharp notches. However, we have successfully applied this method to tungsten, introducing a notch with radius background of about 5–7 μm, which is significantly lower than the grain size of the material, and so that it can be consider almost equivalent to a crack.

3. Results and discussion

3.1. Density and hardness

As shown in Table 2, sample density is similar in all cases. Nevertheless, a small difference appears in the W-alloy with 1 wt%

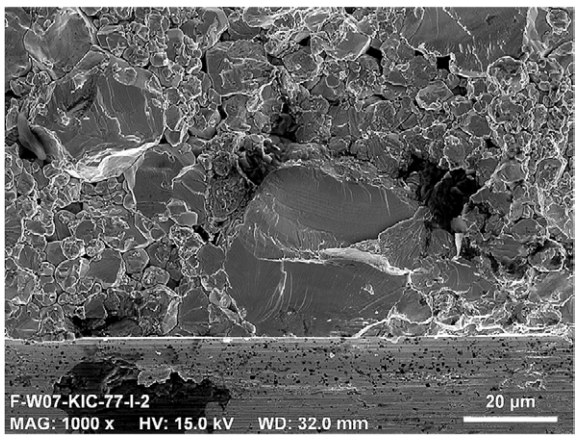

Fig. 3. Notch tip without plastic damage obtained by razor blade notching.

La_2O_3. Results for the different hardness tests are provided in Table 2 and Fig. 4. In all materials, a slight dependence on the applied load is observed; however, this dependence is not relevant if standard deviation of error is considered, because the measurements in most cases are overlapping. An increase in hardness can be clearly seen with the addition of V; values are double those of pure-W, reaching 6 GPa. Although the addition of La_2O_3 does not improve the behavior of the alloy, the mixture of both alloying elements increases the hardness to 7 GPa. If the density of the materials is taken into account, then the alloys with lower density have lower hardness values.

3.2. Modulus of elasticity

Table 3 and Fig. 5 show that results obtained through both techniques are similar; a small discrepancy is apparent in W–4V–1La_2O_3, but the rest of the errors are overlapping. Materials with V content have increased modulus of elasticity; however, these changes are similar to pure-W used by reference (i.e., around 350 GPa). On the other hand, the modulus of elasticity in the alloy with 1La_2O_3 decreased to 270 GPa.

3.3. Fracture toughness

In most cases, load–displacement curves, from the TPB tests, were linear until fracture. Fracture toughness was computed from the maximum load and the initial notch length in each test using the appropriate expression for the stress intensity factor [7]. Toughness values were plotted as function of the temperature as shown in Fig. 6 where the continuous lines and full symbols represent the linear elastic behavior (fracture toughness) and the open symbols represent the plastic behavior (apparent fracture toughness). Results displayed show that materials with V exhibited similar behavior at room temperature, with toughness over 1.5 times higher than the reference W (almost twice for W–4V–1La_2O_3). The toughness for these materials appeared to attain the highest values between 673 and 873 K, decreasing beyond 873 K. This

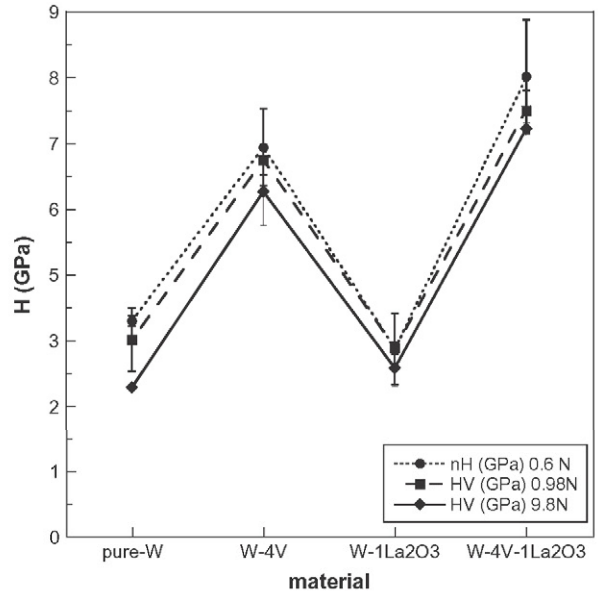

Fig. 4. Average hardness of the samples. Vickers microhardness (HV) with two different applied loads and nanohardness (nH) obtained with instrumented nanoindentation tests.

Table 3
Average elastic modulus values measured with IET and nanoindentation for studied alloys.

Material	E_0 IET (GPa)	nE (GPa)
W	338.0 ± 5.0	346.6 ± 43.2
W–4V	363.5 ± 2.9	385.8 ± 23.4
W–1La_2O_3	269.0 ± 5.5	278.2 ± 22.1
W–4V–1La_2O_3	352.1 ± 0.9	388.3 ± 19.8

behavior is due to accelerated oxidation of the W–V alloys above 873 K, because additions of V to W-alloys cause accelerated oxidation.

Fracture toughness at room temperature for W–1La_2O_3 alloy was similar (except for at low temperature) to pure-W. The La_2O_3 addition does not appear to contribute to the toughness of this material. The differences at 1273 K are not relevant due to oxidation of the reference pure-W at this temperature. It is worthwhile to mention that the W–4V–1La_2O_3 alloy exhibited the best values for fracture toughness at 1273 K. This is due to the toughening effect of the V and the presence of 1 wt% La_2O_3, which limits the oxidation and degradation of the alloy at high temperatures. Fracture toughness is maximum at 673 K with 15 MPa $m^{1/2}$ for this W-alloy.

3.4. Flexural strength

Through force–displacement data obtained in the tests and standard strength of materials formulas [8], σ–ε curves were

Table 2
Experimental (ρ_{exp}), theoretical (ρ_{th}) and relative (ρ_r) density of the samples calculated as can be found in Ref. [3]. Vickers hardness measured with two loads 0.98 and 9.8 N (H_V), nanohardness measured by nanoindentation test (nH) and a load of 0.6 N.

Material	ρ_{exp} (g/cm^3)	ρ_{th} (g/cm^3)	ρ_r (%)	H_V (GPa)$_{0.98\ N}$	H_V (GPa)$_{9.8\ N}$	nH (GPa)$_{0.6\ N}$
W	17.64 ± 0.02	19.25 ± 0.02	91.64	3.40 ± 0.54	2.58 ± 0.03	3.72 ± 0.09
W–4V	17.57 ± 0.02	17.73 ± 0.02	99.10	6.47 ± 0.25	5.94 ± 0.58	6.69 ± 0.66
W–1La_2O_3	17.06 ± 0.09	18.83 ± 0.02	90.60	3.26 ± 0.10	2.91 ± 0.31	3.24 ± 0.61
W–4V–1La_2O_3	17.15 ± 0.04	17.37 ± 0.02	98.73	7.32 ± 0.35	7.01 ± 0.10	7.90 ± 0.97

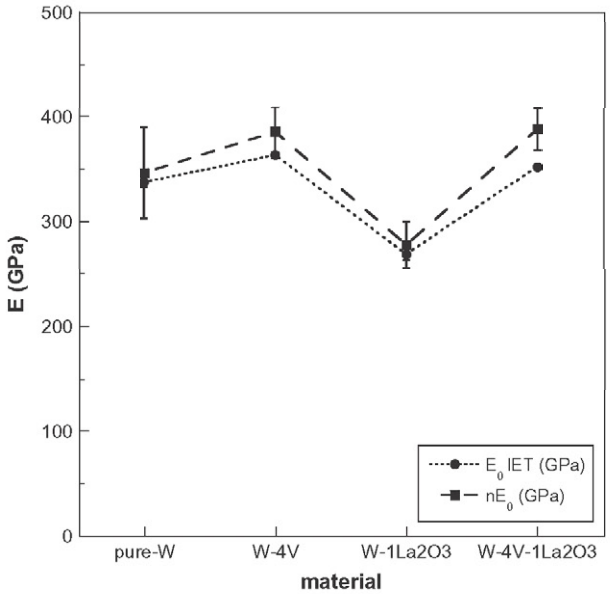

Fig. 5. Average elastic modulus of each material measured by IET and nanoindentation tests.

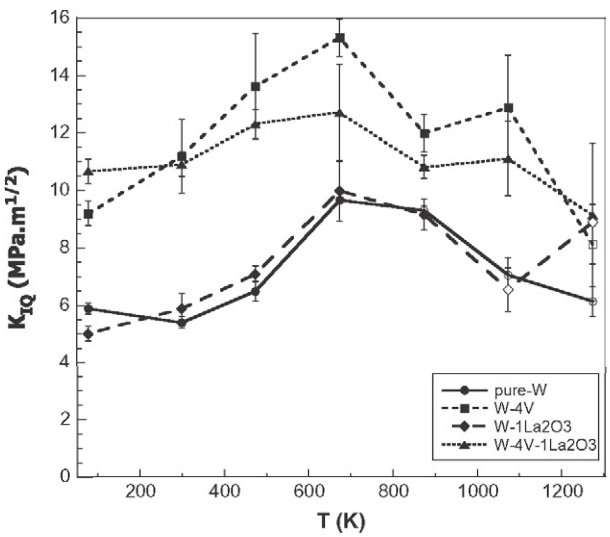

Fig. 6. Average fracture toughness versus test temperature for each material. Open symbols represent the apparent fracture toughness.

plotted and used to determine the maximum tensile strength in bending. However, this method is restricted to elastic bending and at high temperatures these materials become plastic. Therefore, the 0.2% yield strength offset was used when ductile behavior was observed. These data are shown in Fig. 7, with the 0.2% yield strength represented with dashed lines and open symbols.

Fig. 7 shows that pure-W exhibits a small increase in strength between 298 and 473 K, but then the strength decreases due to thermal degradation; its ductile to brittle transition temperature (DBTT) is between 473 and 673 K.

Even at low temperatures, the W–4V alloy exhibits higher strengths compared to those of pure-W. W–V exhibits a linear elastic behavior up to 1073 K, which is why its DBTT is between 1073 and 1273 K. W–4V reaches a maximum strength of about 580 MPa at 873 K and at higher temperatures the measured strength decreased due to severe oxidation, which is extremely severe at

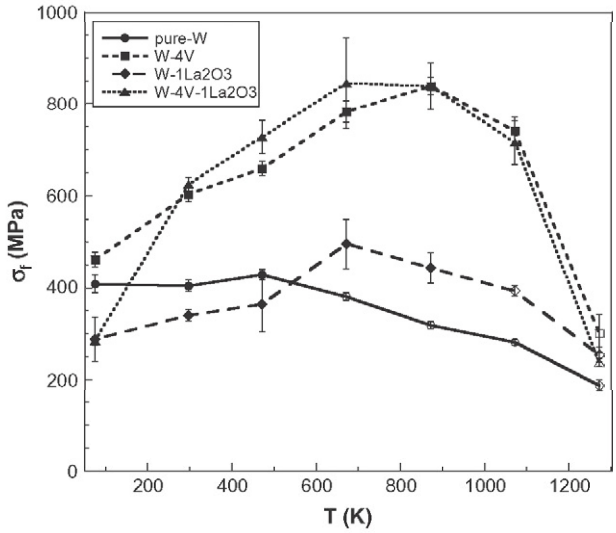

Fig. 7. Average flexure strength versus test temperature of each material. Open symbols represent the yield strength at 0.2%.

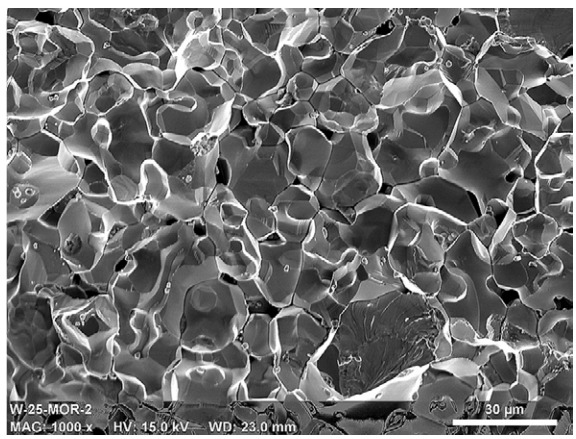

Fig. 8. Fracture surface at 298 K of pure-W.

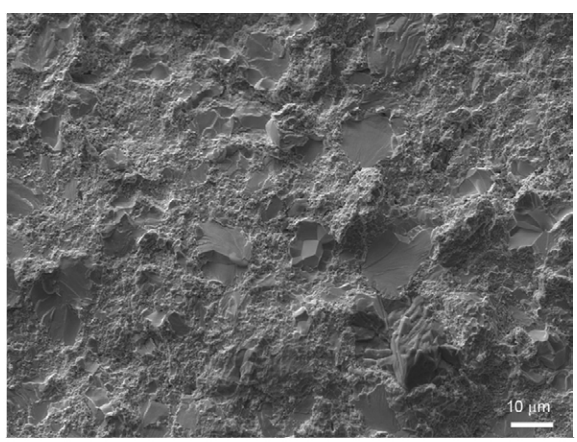

Fig. 9. Fracture surface at 298 K of W–4V.

1073 K and above. Its behavior with temperature is consistent with that found for the fracture toughness. Flexural strength increased around the DBTT, and underwent subsequent degradation due to the oxidation of the material and to the development of plastic failure processes. It should be noted that the flexural strength of the

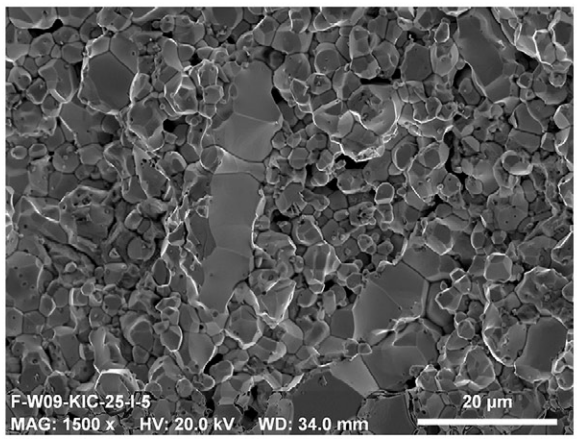

Fig. 10. Fracture surface at 298 K of W–1La_2O_3.

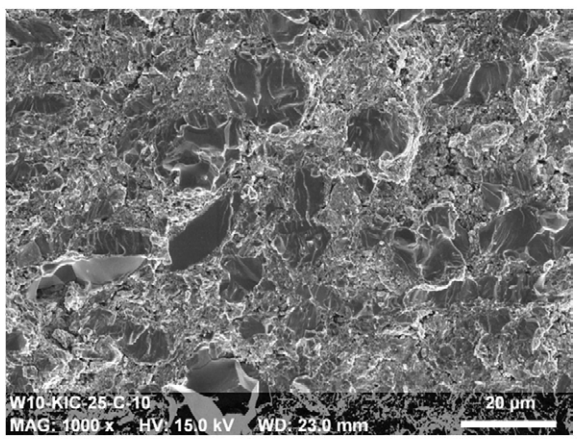

Fig. 11. Fracture surface at 298 K of W–4V–1La_2O_3.

W–4V or W–4V–1La_2O_3 alloys are quite similar in all the cases to pure-W, with a maximum (around 850 MPa) at 873 K (roughly 3 times higher the strength of the reference W at the same temperature).

The strength of the W–1La_2O_3 alloy is a little lower than of W below 473 K. Above this temperature its strength increases slightly, but not significantly.

3.5. Fracture surfaces

Fracture surfaces for all alloys were flat with brittle fracture features, consistent with the macroscopic results obtained from the σ–ε curves (Figs. 6 and 7). No plastic deformation was observed according to the fracture surface observations.

Two types of surfaces were observed. Pure-W (Fig. 8) and W–1La_2O_3 (Fig. 10), showed more porosity between the grains. No mixture of the alloying elements was observed; therefore, no solid solution formed to the cohesion to the material. For this reason these materials have inferior mechanical properties. In general, this failure is due to a grain boundary decohesion process. As shown in Fig. 10, elongated grains may form during the fabrication process. Conversely, some V-containing alloys (Figs. 9 and 11) formed a solid solution of W–V surrounding the larger grains, giving greater grain boundary cohesion, which improves mechanical properties. The majority of the fracture surfaces reveal intergranular fracture, but the larger grains reveal transgranular cleavage fracture.

4. Conclusions

The addition of V reduced porosity and produced a significant increase in both strength and fracture toughness compared to pure-W. The maximum values achieved for flexural strength and fracture toughness were 850 MPa at 873 K and 15 MPa $m^{1/2}$ at 673 K, respectively. In addition, V additions retarded the onset of oxidation, but when it occurred, oxidation was observed to occur to a greater extent. An increase of the DBTT kept the brittle behavior at temperatures above 1073 K. However, the mechanical properties remained higher than those of pure-W.

The addition of La_2O_3 reduced the densification of the samples, thus no significant improvement in the mechanical properties was noted. The DBBT increased at temperatures above 873 K, which is lower than with W–4V.

The combined effect of alloying W with V and La_2O_3 produced a high densification of the material with the highest hardness value (7.5 GPa). The mechanical strength was high, similar to W–4V, but more brittle, so the fracture toughness value was lower. Furthermore, an increase was observed in DBTT to temperatures above 1073 K.

As for the new technique developed for introducing the notch, no damage was observed by plastic deformation in the grains around the notch tip. In addition, a notch tip with a radius about 5–7 μm, was obtained. This value is significantly lower than the material grain size and therefore we are confident that the value of fracture toughness is independent of the notch root radius.

Acknowledgments

This investigation was supported by Comunidad de Madrid (S-S2009/MAT-1585), EFDA-ITER (WP12-MAT-W ALLOY), Ministerio de Economía y Competitividad of Spain (ENE2012-39787-C06-05 and MAT2012-38541-c02-02). TEM measurements have been made at LABMET, TEM Laboratory associated to the Red de Laboratorios de la Comunidad de Madrid.

References

[1] G. Federici, Nucl. Fusion 41 (12R) (2001).
[2] F. Druyts, J. Fays, C.H. Wu, Fusion Eng. Des. 63–64 (2002) 319–325.
[3] A. Muñoz, M.A. Monge, B. Savoini, M.E. Rabanal, G. Garces, R. Pareja, J. Nucl. Mater. (2011).
[4] Standard test method for dynamic Young's modulus, shear modulus, and Poisson's ratio for advanced ceramics by impulse excitation of vibration, ASTM C1259-98, Annual Book of ASTM Standards, American Society for Testing and Materials, West Conshohocken, Pennsylvania 15.01, 1999, pp. 386–400.
[5] W.C. Oliver, G.M. Pharr, J. Mater. Res. 7 (6) (1992).
[6] T. Nose, T. Fujii, Am. Ceram. Soc. 71 (5) (1988) 328–333.
[7] G.V. Guinea, J.Y. Pastor, J. Planas, M. Elices, Int. J. Fract. 89 (2) (1998).
[8] S. Timoshenko, Strength of Materials, third ed., D. Van Nostrand Company, 1955.